Supplementary Material for
Quantum network of atom clocks: a possible implementation with neutral atoms

P. Kómár,[1] T. Topcu,[1, 2, 3] E. M. Kessler,[1, 3] A. Derevianko,[1, 2, 3] V. Vuletić,[4] J. Ye,[5] and M. D. Lukin[1]

[1]*Physics Department, Harvard University, Cambridge, MA 02138, USA*
[2]*Department of Physics, University of Nevada, Reno, NV 89557, USA*
[3]*ITAMP, Harvard-Smithsonian Center for Astrophysics, Cambridge, MA 02138, USA*
[4]*Department of Physics and Research Laboratory of Electronics,*
Massachusetts Institute of Technology, Cambridge, MA 02139, USA
[5]*JILA, NIST, Department of Physics, University of Colorado, Boulder, CO 80309, USA*
(Dated: May 30, 2016)

I. USING THE MESSENGER ATOM

With proper optical control, we can entangle the ensembles by moving a single Rydberg atom to the vicinity of each ensemble sequentially, such that its blockade radius covers one of the clouds entirely. Starting from the state

$$|g\rangle^{nM}\big(|s\rangle + |r_2\rangle\big), \tag{1}$$

where the first nM ket stand for the state of all atoms in the M ensembles (each having n atoms), and the last one represents the state of the messenger atom. In a sequence, we imagine the messenger atom to be brought to the vicinity of each ensemble, and the pulse sequence $[\pi/\sqrt{N}]_{g,r1}, [\pi]_{f,r1}$, creates an f excitation, conditioned on the state of the messenger atom. This plays out as follows

$$\rightarrow |g\rangle^{n(M-1)}\big(|1_f\rangle_1|s\rangle + |0\rangle_1|r_2\rangle\big) \tag{2}$$

$$\rightarrow |g\rangle^{n(M-2)}\big(|1_f\rangle_1|1_f\rangle_2|s\rangle + |0\rangle_1|0\rangle_2|r_2\rangle\big) \tag{3}$$

$$\vdots \tag{4}$$

$$\rightarrow \big(|1_f\rangle^M|s\rangle + |0\rangle^M|r_2\rangle\big), \tag{5}$$

which then only requires the messenger atom to be measured in the $|\pm\rangle = (|s\rangle \pm |r_2\rangle)$ basis, resulting in

$$\rightarrow |1_f\rangle^M \pm |0\rangle^M, \tag{6}$$

the required entangled state before the final GHZ extension step.

Disregarding the technical difficulties of trapping multiple atomic ensembles in the same vacuum chamber, this entangling method has a higher fidelity than the previous, photon-based, protocol, since it does not suffer from the errors affecting the photon emission, propagation and detection. We model the imperfections of this scheme by summing the error terms $\varepsilon_1 + \varepsilon_2 + \varepsilon_3$ only (from Eq. (11), (14), (16)).

In section XI, we calculate a more accurate result for the error contribution of imperfect blockade in the case of placing the messenger atom close on the border of the cloud. We find that this increases the effect of the imperfect blockate by a factor of ~ 2, resulting in an increase of $\sim 10\%$ in the total error.

II. OVERVIEW OF OPTIMIZATION

In section VII, we show that the figure of merit, the precision gain with respect to non-entangled schemes, can be written as

$$G(N, E) = \frac{\pi}{8}e^{-EN}\sqrt{\frac{N}{\log N}}, \tag{7}$$

where N is the total number of entangled atoms in the global GHZ state, and $E = E(n, \Omega)$ is the total error (contrast loss) divided by the total number of atoms. E depends on the number of atoms at a single clock, n, and the Rabi-frequency of the dressing field used for local entanglement growing.

We separate out the minimization of E (through finding the optimal n, Ω parameters), and the maximization of G (through finding the optimal N). In other words, we find

$$G_{\max} = \max_N G\left(N, \min_{n,\Omega} E\right). \tag{8}$$

This two-step procedure gives identical results to the full optimization,

$$G_{\max} = \max_{N,n,\Omega} G\big(N, E(n, \Omega)\big), \tag{9}$$

because both the maximum of G and the optimal value of N are monotonically decreasing functions of E, for large N (as can be seen from Eq. (7)). We choose the two-step procedure because it is easier to carry out and interpret.

III. LOCAL ENTANGLING ERRORS

The initial GHZ state is never perfect due to a series of imperfections in the implementation. Here, we analyze the main errors responsible for lowering the initial fidelity $F_{\text{local}} = [1 + \exp(-\varepsilon_{\text{local}})]/2$ of the GHZ state of n atoms, created via the conditional dressing scheme, described in the main article. We assume the following errors to be independent and small, and we approximate $\varepsilon_{\text{local}}$ with the sum of the individual errors, $\sum_j \varepsilon_j$. We evaluate the errors for a 2D square lattice filled in a circular region

and a 3D cubic lattice filled in a spherical region (both of radius R). Where there is a difference between the two cases, we give both results.

A. Imperfect blockade

If the blockade between the levels r_1 and r_2, Δ_{12}, is not large enough, the population transfer $g \to f$ happens even if r_2 is populated by a single atom. Here, we analyze the effect of this imperfection.

Each pulse $\left[\frac{\pi}{\sqrt{n-j+1}}\right]_{g,r1}$, for $j = 1, 2, \ldots n$ excites an average population of $\sim n\left(\frac{\Omega}{2\Delta_{12}}\right)$ to the r_1 Rydberg state even if it is detuned by Δ_{12} due to the interaction with the control atom being in r_2 state. There are n such pulses total, resulting in the error

$$\varepsilon_1 = \frac{n^2\Omega^2}{4}\left\langle\frac{1}{\Delta_{12}^2}\right\rangle, \tag{10}$$

where the average is taken over every pair of atoms in the ensemble. After calculating this average for 2D and 3D spherical ensembles with uniform density, we obtain

$$\varepsilon_1 = \left(\frac{\hbar a^3\Omega}{C_{12}^{(3)}}\right)^2 \times \begin{cases} 0.02818\,n^5 & \text{(2D)} \\ 0.06079\,n^4 & \text{(3D)} \end{cases}, \tag{11}$$

where $C_{12}^{(3)}$ is the dipole-dipole coefficient of the interaction between r_1 and r_2, and a is the lattice constant of the square (cubic) lattice of the 2D (3D) ensemble.

B. Decaying Rydberg states

During the pulse sequence that induce the population transfer from g to f, the r_1 level is populated by an average of $1/2$ atoms. With constant Ω Rabi frequency, the times of the pulse j is $\frac{\pi}{\Omega\sqrt{j}}$. The total accumulated error during the pulse sequence due to decay or dephasing of r_1 Rydberg state is

$$\varepsilon_2^{(1)} = \frac{\gamma_1}{2}\frac{\pi}{\Omega}2\sum_{j=1}^{n}\frac{1}{\sqrt{j}} \approx \gamma\sqrt{n}\frac{2\pi}{\Omega} \tag{12}$$

where γ_1 is the total rate of loss (environment induced decay and dephasing) from the Rydberg level r_1. The additional factor of 2 appears because both the $g \to r_1$ and $r_1 \to f$ transfers need to happen.

In the meantime, the r_2 level is populated by a single atom. The decay and dephasing of r_2, which we assume to be happening with rate γ_2 causes error accumulation, which we approximate as

$$\varepsilon_2^{(2)} = \gamma_2\frac{\pi}{\Omega}2\sum_{j=1}^{n}\frac{1}{\sqrt{j}} \approx \gamma\sqrt{n}\frac{4\pi}{\Omega}. \tag{13}$$

Although the two errors affect different components of the wavefunction, we use their sum as an upper bound of their effect:

$$\varepsilon_2 = \varepsilon_2^{(1)} + \varepsilon_2^{(2)} = 6\pi\sqrt{n}\frac{\gamma}{\Omega}. \tag{14}$$

C. Imperfect self-blockade

During the excitation of the Rydberg state r_1, double excitations are mostly shifted out of resonance by Δ_{11} due to the strong van der Waals interaction between two r_1 atoms. The time average of the population in the state where one Rydberg atom is excited is $1/2$. The collective Rabi frequency between the 1-Rydberg state and the 2-Rydberg state is $\sqrt{2(n-1)}\Omega$. This translates to an average population of $(n-1)\left(\frac{\Omega}{2\Delta_{11}}\right)$ during a single pulse. Since there are n such pulses during the population transfer from g to f, the total accumulated error is

$$\varepsilon_3 \approx \frac{n^2\Omega^2}{4}\left\langle\frac{1}{\Delta_{11}^2}\right\rangle. \tag{15}$$

After evaluating the average over all pair in the 2D (3D) ensemble, we obtain

$$\varepsilon_3 = \left(\frac{\hbar a^6\Omega}{C_{11}^{(6)}}\right)^2 \times \begin{cases} 0.01594\,n^8 & \text{(2D)} \\ 0.05544\,n^6 & \text{(3D)} \end{cases} \tag{16}$$

where $C_{11}^{(6)}$ is the van der Waals coefficient of the interaction between two r_1 atoms, and a is the lattice constant of the square (cubic) lattice of the 2D (3D) ensemble.

IV. NON-LOCAL ENTANGLING ERRORS

Our protocol requires $K-1$ links to be set up between K clocks. We denote the fidelity of a single connection by $F_{\text{non-local}} = [1 + \exp(-\varepsilon_{\text{non-local}})]/2$, and we approximate $\varepsilon_{\text{non-local}}$ with the sum of individual errors $\sum_i \varepsilon_i$, detailed below.

A. Imperfect blockade

When exciting a single collective excitations, imperfect self-blockade can result in leakage into double excited states. The probability of this can be exponentially reduced by applying a smooth driving pulse. E.g., in case of a Gaussian pulse of width τ, and area π, exciting the $g \to r_1$ transition is expected to be blocked when r_2 is populated, but it succeeds with probability P_{double},

$$P_{\text{double}} \approx \frac{\pi^2}{4}\exp\left[-\frac{(\Delta_{12}\tau)^2}{2}\right], \tag{17}$$

where $\Delta_{12} = C_{12}^{(3)}/(\hbar(2R)^3)$ is the minimal energy shift in the ensemble due to the interaction of two atoms, one

in r_1 and one in r_2. A detailed analysis of how different pulses affect the transition probability can be found in [1]. $P_{\text{double}} \ll 1$ requires

$$\tau \leq \frac{\sqrt{2}}{\Delta_{12}} = \begin{cases} 2n^{3/2} \frac{\hbar a^3}{C_{12}^{(3)}} & (2D) \\ 2.7\, n \frac{\hbar a^3}{C_{12}^{(3)}} & (3D) \end{cases} \qquad (18)$$

in order to be small compared to the other errors.

B. Rydberg state decay

The $g \to r_1$ transition is driven with a pulse of duration τ, during which the r_2 level has a single excitation, which decays with rate γ_2. The resulting error contribution, after all four photon pulses have been generated, is

$$\varepsilon_4 = 4\gamma_2\tau = \begin{cases} 8n^{3/2} \frac{\hbar a^3 \gamma_2}{C_{12}^{(3)}} & (2D) \\ 10.8\, n \frac{\hbar a^3 \gamma_2}{C_{12}^{(3)}} & (3D) \end{cases} \qquad (19)$$

where we used the expressions for τ from Eq. (18).

C. Photon propagation and detection errors

The pairs of photons can get lost in the fiber during propagation and the detection process (which is limited to 50% for time-resolving detectors, and 25% for non-time-resolving ones). The two-photon heralding, however, detects both of these errors. The remaining error comes from dark-counts of the detectors. This affects a single link with the error

$$\varepsilon_5 \approx 4\gamma_{\text{dark}} T_{\text{detect}} = \gamma_{\text{dark}} \frac{20}{n\gamma_e}, \qquad (20)$$

where γ_{dark} is the dark count rate of the detectors, T_{detect} (chosen such that a properly timed detector would have a chance to catch $1 - e^{-5} > 99\%$ of each photon) is the "open time" of the detector, and γ_e is the spontaneous emission lifetime of the $|e\rangle \to |g\rangle$ transitions. The factor of n is due to the collective enhancement of the said transition, and the factor of 4 is because four pulses are used in each connection.

We note that the probabilistic nature of the two-photon detection requires repeating the connection steps between clocks every time it fails. With no additional noise, this happens every second time, on average, requiring resetting the f and s qubits in the two clocks in question. If the distance between clocks is very large, photon propagation errors will increase the average number of resets required for a single connection. Since every qubit reset introduces additional errors, we want to minimize photon loss. If the photon loss probabilit is ε, the two-photon coincidence probabilit becomes $\frac{1}{2}(1-\varepsilon)^2$.

In the case of optical fibers (using an attenuation length of $L_{\text{att}} \sim 20$ km), we estimate $\varepsilon \sim 1 - e^{-L/L_{\text{att}}}$, whose effect becomes comparable to the ideal 50% chance

at around $L \sim 7$ km. Currently we imagine our scheme working for terrestrial labs connected by fiber not longer than this.

If clocks are operational on board of satellites, and optical links are establised by actively stabilized telescopes, we estimate the photon loss probability, due to diffraction, using the far-field (normalized) intensity distribution (Airy-disk), $P(\theta) = \frac{1}{\pi} \left(\frac{J_1(kR\sin\theta)}{\sin\theta} \right)^2$, where J_1 is a Bessel function. After approximating $\sin\theta \approx \theta$, we can write the photon error probability as

$$\varepsilon = 1 - 2 \int\limits_0^{kR^2/L} dx\, \frac{(J_1(x))^2}{x}, \qquad (21)$$

where R is the radius of the telescope objectives, and k is the photon's wavevector. Assuming $R \sim 1.25$ m (Hubble's objective) and 3.11 eV photon, the distance when photon loss error rate reaches 50% is 1.5×10^7 m $= 15,000$ km, which is larger that the average distance between neighboring GPS satellites.

D. Memory loss

During the creation step of each link, the state $|s\rangle$ is used as memory. On average, every link relies on one s qubit. The time it takes to attempt the creation of a link is $\sim 2L/c$, the time it takes for a light pulse to do a round-trip between two stations. During this time, quantum information is stored in qubit s, which is subject decoherence happening at a rate γ_s. The infidelity of the link originating from this error is

$$\varepsilon_6 = 4\frac{2L}{c}\gamma_s. \qquad (22)$$

State $|f\rangle$ is assumed to be a long-lived clock state, its decoherence rate is negligible.

E. Imperfect photon collection

Collective enhancement makes the excited atom in state $|e\rangle$ decay preferentially to $|g\rangle$, and emit a photon directly to the spatial mode $\mathbf{k}_e$, where $\mathbf{k}_e$ is the spatial frequency of the collective mode e. In the implementation with Yb atoms (discussed in Section V), the decay channel to $|g\rangle$ has a close to unity branching ratio ($\zeta = 0.99$), but due to the finite size of the ensemble, the photon collection efficiency is decreased. The probability of not capturing the emitted photon is

$$\varepsilon_7 \approx \frac{k_e^2 w^2}{3nI} = \begin{cases} \frac{k_e^2 a^2}{3\pi I}; & (2D) \\ \frac{k_e^2 a^2}{3n^{1/3} I} \left(\frac{3}{4\pi}\right)^{2/3}, & (3D) \end{cases} \qquad (23)$$

where w is the radius of the ensembles cross section perpendicular to $\mathbf{k}_e$, ($w = a(n/\pi)^{1/2}$ for 2D, and $w =$
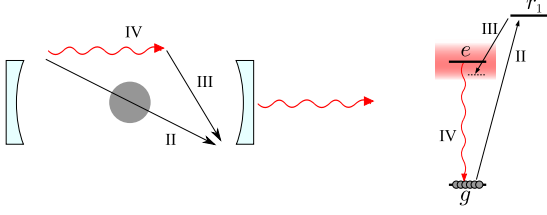
FIG. 1. The spontaneous emission can be enhanced by an optical cavity only if the fields involved in the process are phase matched. This is possible by setting the setting the frequence of field III slightly higher, allowing the three fields to not be co-propagating. This way the coherent fields can enter at an angle, and not be blocked by the high-finesse optical cavity. The transition rate does not change considerably if the detuning of III is smaller than the linewidth of level e.

$a(3n/(4\pi))^{1/3}$ for 3D.), and $k_e = 2\pi/(1.4\,\mu\text{m})$, and $I \sim 100$ is the finesse of the cavity that we envision using.

We note that in order to take full advantage of the collective enhancement factor, n in Eq. (23), the phase matching condition has to be satisfied between the two coherent fields, $g \to r_1$ (II) and $r_1 \to e$ (III), and the spontaneously emitted photon $e \to g$ (IV). When an optical cavity is placed around the ensemble, for the purpose of enhancing the spontaneous emission, one need to carefully choose the wavevectors of field II and III, such that $\mathbf{k}_{\text{IV}} = \mathbf{k}_{\text{II}} - \mathbf{k}_{\text{III}}$, where $\mathbf{k}_{\text{IV}}$ is the wavevector of the emitted photon, which should be paralell to the axis of the optical cavity, and the fields II and III should be incident at a non-zero angle in order to not be blocked by the cavity. This is possible only if the magnitude of $\mathbf{k}_{\text{III}}$ is chosen to be slightly larger than required to bridge the energy difference between r_1 and e. Because the frequency of the state e has a large spread (since it is very short-lived), the rate of the $r_1 \to e \to g$ transition will not change significantly. (See Fig. 1.)

V. IMPLEMENTATION WITH YB

We imagine using the lower levels of neutral Yb for our protocol, $|g\rangle = |6s^2(^1S_0)\rangle$, $|f\rangle = |6s6p(^3P_0)\rangle$, $|s\rangle = |6s6p(^3P_2)\rangle$ and $|e\rangle = |6s6p(^1P_1)\rangle$, and two Rydberg levels $|r_1\rangle = |6s\tilde{n}p_{m=+1}(^1P_1)\rangle$ and $|r_2\rangle = |6s\tilde{n}s(^3S_1)\rangle$ with the same principle quantum number $\tilde{n}$. In the case of the 2D lattice, we set the quantization axis perpendicular to the plane in which the atoms reside, this way the dipole-dipole interaction between two atoms, one in $|r_2\rangle$ and the other in $|r_1\rangle$, depends only on their separation, $|\mathbf{r}_1 - \mathbf{r}_2|$. In the case of the 3D lattice, we rely on the overwhelming strength of the Rydberg interaction to produce reliable blockade even between atoms in different horizontal planes.

A. Rydberg lifetimes

We use the measured values from [2] for principle quantum numbers $\tilde{n} \sim 20 - 30$, and extrapolate the inverse lifetimes of the Rydberg states

$$\gamma_1 \approx \gamma_2 = \gamma = \frac{8.403 \times 10^8 \text{ s}^{-1}}{(\tilde{n} - 4.279)^3} \quad (24)$$

where $\tilde{n}$ is the principle quantum number of the Rydberg orbit. Although the measurement was carried out at 300 K, the contribution of the black body radiation (at $\tilde{n} \sim 20 - 30$) is negligible even at this temperature, and therefore our extrapolation accurately describes the effect of spontaneous emission on the lifetime. Cooling of the radiation environment will be necessary to reach the above lifetime at $\tilde{n} \sim 100$ and above. Furthermore, the photoionization rate from the $\tilde{n} = 120$ Rydberg level, in a trapping field with 10^4 W/cm^2 intensity, is five times smaller ($\gamma_{\text{PI}} \sim 110$ s^{-1}), than the natural liftime ($\gamma \sim 540$ s^{-1}).

B. Self-blockade, Δ_{11}

The long-range interaction between two r_1 atoms at a distance R is dominated by the van der Waals potential,

$$\Delta_{11}(R) = \frac{C_{11}^{(6)}}{\hbar R^6}, \quad (25)$$

where $C_{11}^{(6)}$ strongly depends on the principle quantum number $\tilde{n}$. We use results from [3], and extrapolate the $C_{11}^{(6)}$ coefficient to high principle quantum numbers with the following formula,

$$C_{11}^{(6)} = (-0.116 + 0.0339\,\tilde{n})\,\tilde{n}^{11} \text{ a.u.} \quad (26)$$

where the a.u. stands for atomic units, $E_h a_0^6 = 9.573 \times 10^{-80}$ Jm^6, where E_h is the Hartree energy and a_0 is the Bohr radius.

C. Cross-blockade, Δ_{12}

The long-range interaction between an r_1 and an r_2 atoms at a distance R is dominated by the dipole-dipole interaction. We assume that the atoms are confined in the xy plane, and because the $6s\tilde{n}p_{m=+1}$ state is polarized in the z direction, the interaction strength is independent of the relative direction of one atom to the other.

$$\Delta_{12}(R) = \frac{C_{12}^{(3)}}{\hbar R^3}, \quad (27)$$

where $C_{12}^{(3)}$ depends strongly on the principle quantum number $\tilde{n}$. We use results from [3], and extrapolate the

$C_{12}^{(3)}$ coefficient to high principle quantum numbers with the following formula,

$$C_{12}^{(3)} = (0.149 + 0.00077\,\tilde{n})\,\tilde{n}^4 \text{ a.u.} \qquad (28)$$

where the a.u. stands for atomic units, $E_h a_0^3 = 6.460 \times 10^{-49}$ Jm^3.

D. Decay rates of lower levels

The decay rate of $|s\rangle = |6s6p\,,^3P_2\rangle$ is $\gamma_s = [14.5\,\mathrm{s}]^{-1} = 0.069\,\mathrm{s}^{-1}$. The decay rate of the excited state $|e\rangle = |6s6p\,,^1P_1\rangle$ is $\gamma_e = 1.8 \times 10^8\,\mathrm{s}^{-1}$.

E. Photon channels

We assume that neighboring stations are $L < 10\,\mathrm{km}$ apart from each other, we neglect fiber and coupling loss. We further assume that single photon detectors have a low dark count rate, i.e. $\gamma_{\mathrm{dark}} \approx 10\,\mathrm{s}^{-1}$.

VI. OPTIMIZATION

The total initial imperfections of a GHZ state with N atoms divided into K clocks, each enclosing M equal-sized ensembles (each of which contain n atoms) is

$$\varepsilon_{\mathrm{tot}} = (K-1)\varepsilon_{\mathrm{non\text{-}local}} + MK\varepsilon_{\mathrm{local}} \qquad (29)$$

$$\approx N\left(\frac{\varepsilon_{\mathrm{local}}}{n} + \frac{\varepsilon_{\mathrm{non\text{-}local}}}{Mn}\right) =: NE, \qquad (30)$$

where the error contributions are $\varepsilon_{\mathrm{local}} = \varepsilon_1 + \varepsilon_2 + \varepsilon_3$, and $\varepsilon_{\mathrm{non\text{-}local}} = \varepsilon_4 + \varepsilon_5 + \varepsilon_6 + \varepsilon_7$, from Eq. (11, 14, 16, 19, 20, 22 and 23).

It is clear that the larger M is, the smaller the error is, however nM (the number of atoms in a single clock) is limited by the current state of technology to $(nM)_{\mathrm{opt}} \sim 2500$. Independently from the total atom number, N, there is an optimal ensemble size, n_{opt}, for which E (the total error per atom) is minimal. Below we find the optimal values of the parameters Ω, (the Rabi frequency the population transfer), and n (the size of the each ensemble) for fixed values of $\tilde{n}$ (the principle quantum number of the Rydberg state) and $a = 275.75\,\mathrm{nm}$.

Using the following dimensionless variables, $\omega = \Omega/\gamma$, $\delta_{11} = \frac{C_{11}^{(6)}}{\hbar a^6 \gamma}$ and $\delta_{12} = \frac{C_{12}^{(3)}}{\hbar a^3 \gamma}$, we can write the error per atom as $E := \sum_i e_i$, where the terms are $e_i = \varepsilon_i/n$ for $i =$

$1, 2, 3$ and $e_i = \varepsilon_i/(Mn)_{\mathrm{opt}} = \varepsilon_i/2500$ for $i = 4, 5, 6, 7$,

$$e_1 = \left(\frac{\omega}{\delta_{12}}\right)^2 \times \begin{cases} 0.02818\,n^4 & (2\mathrm{D}) \\ 0.06079\,n^3 & (3\mathrm{D}) \end{cases} \qquad (31)$$

$$e_2 = \frac{6\pi}{n^{1/2}\omega} \qquad (32)$$

$$e_3 = \left(\frac{\omega}{\delta_{11}}\right)^2 \times \begin{cases} 0.01594\,n^7 & (2\mathrm{D}) \\ 0.05544\,n^5 & (3\mathrm{D}) \end{cases} \qquad (33)$$

$$e_4 = \frac{1}{\delta_{12} \times 2500} \times \begin{cases} 8\,n^{3/2} & (2\mathrm{D}) \\ 10.8\,n & (3\mathrm{D}) \end{cases} \qquad (34)$$

$$e_5 = 7.6 \times 10^{-5}\,\frac{1}{2500 \times n} \qquad (35)$$

$$e_6 = 1.8 \times 10^{-5}/2500 \qquad (36)$$

$$e_7 = \frac{1.532}{3 \times 10^2 \times 2500} \times \begin{cases} \frac{1}{\pi} & (2\mathrm{D}) \\ \frac{1}{n^{1/3}}\left(\frac{3}{4\pi}\right)^{2/3} & (3\mathrm{D}) \end{cases} \qquad (37)$$

A. Optimal parameters

We numerically minimized the sum, $E = \sum_i e_i$, by finding the optimal values of n for every $\tilde{n} \in [50, 150]$, for $\omega = 10^5$. (For $\tilde{n} = 120$, this Rabi frequency, $\Omega = 10^5\gamma = 5.42 \times 10^7\,\mathrm{s}^{-1}$ is small enough, that the nearest neighboring Rydberg level is well out of resonance: The level spacing is ~ 30 GHz between the $6s120s$ and $6s119s$ levels.)

The optimal number of atoms at a single ensemble n_{opt} are shown on Fig. 2.
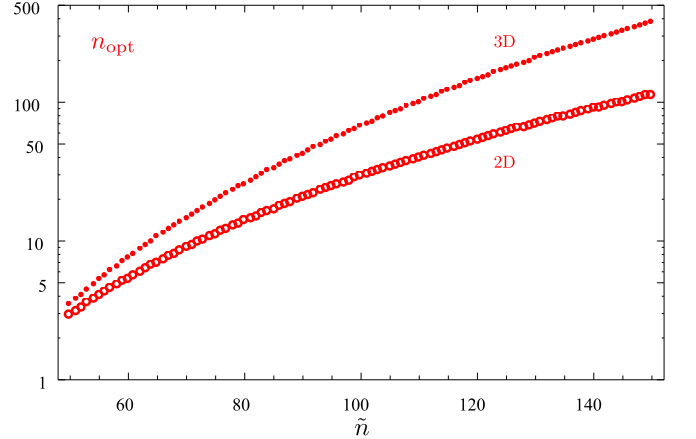
FIG. 2. The optimal number of atoms in a single ensemble n is plotted as a function of the principle quantum number of the Rydberg levels $\tilde{n}$, for the 2D and 3D setup.

The minimal error per atom E_{min} is shown on Fig. 3 as a function of $\tilde{n}$.

B. Comparison of error sources

We compare the contributions of the different error terms e_i to the total error per atom, $\sum_i e_i$, for $\tilde{n} = 120$.
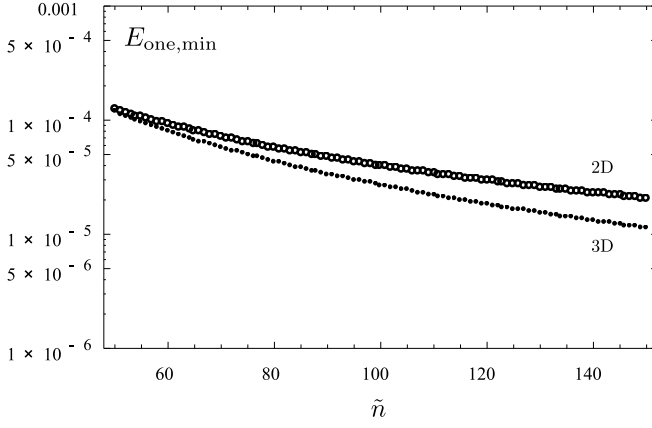
FIG. 3. The minimized error contribution of a single atom as a function of the principle quantum number of the Rydberg levels $\tilde{n}$, for the 2D and 3D setup.

Errors in 2D ensemble	error per atom	ratio in total
imperfect blockade (e_1)	3.2×10^{-6}	11%
Rydberg decay (e_2)	2.5×10^{-5}	87%
self-blockade (e_3)	$\sim 10^{-10}$	< 0.1%
r_2 decay (non-local) (e_4)	$\sim 10^{-11}$	< 0.1%
photon detection (e_5)	$\sim 10^{-12}$	< 0.1%
memory error (e_6)	$\sim 10^{-9}$	< 0.1%
photon collection (e_7)	6.5×10^{-7}	2%
total error per atom	3.0×10^{-5}	100%

TABLE I. The absolute and relative contribution of the different error sources to the total error per atom at $\tilde{n} = 120$, $\Omega = 10^5 \gamma$ and $n = n_{\text{opt}} = 54$.

The different error terms contribute to the sum with amounts given in Table I and II.

VII. CLOCK PRECISION

A. Imperfect initialization

The precision of an atomic clock employing a GHZ state of N clock atoms is limited by the initial imperfect creation of the GHZ state described by the fidelity F_N

Errors in 3D ensemble	error per atom	ratio in total
imperfect blockade (e_1)	2.6×10^{-6}	14%
Rydberg decay (e_2)	1.6×10^{-5}	86%
self-blockade (e_3)	$\sim 10^{-11}$	< 0.1%
r_2 decay (non-local) (e_4)	$\sim 10^{-11}$	< 0.1%
photon detection (e_5)	$\sim 10^{-12}$	< 0.1%
memory error (e_6)	$\sim 10^{-8}$	< 0.1%
photon collection (e_7)	$\sim 10^{-8}$	< 0.1%
total error per atom	1.8×10^{-5}	100%

TABLE II. The absolute and relative contribution of the different error sources to the total error per atom at $\tilde{n} = 120$, $\Omega = 10^5 \gamma$ and $n = n_{\text{opt}} = 146$.

or contrast $c = 2F_N - 1$. We assume that an imperfect creation of the GHZ state result in the density matrix

$$\rho_{\text{non-pure}} = c|\Psi\rangle\langle\Psi| + \frac{1-c}{2}\big(|\mathbf{0}\rangle\langle\mathbf{0}| + |\mathbf{1}\rangle\langle\mathbf{1}|\big), \quad (38)$$

where $|\Psi\rangle = \frac{|\mathbf{0}\rangle + |\mathbf{1}\rangle}{\sqrt{2}}$, $|\mathbf{0}\rangle = |0\rangle^{\otimes N}$, $|\mathbf{1}\rangle = |1\rangle^{\otimes N}$, and we assumed that only the relative phase between the two components of the GHZ state changes to an unknown value, but no relaxation happens.

B. Measurement

After the interrogation time, the two components of the GHZ state pick up a relative phase $N\phi$. $|\Psi\rangle \rightarrow |\Psi_\phi\rangle = [|\mathbf{0}\rangle + e^{iN\phi}|\mathbf{1}\rangle]/\sqrt{2}$. Performing a perfect single-atom $-\pi/2$ rotation around the y axis for all atoms transforms this into

$$|\Psi'_\phi\rangle = \frac{1}{\sqrt{2^{N+1}}} \sum_{\{q_j\}} \left[1 + (-1)^{\sum_j q_j} e^{iN\phi}\right] |q_1, q_2, \ldots q_N\rangle,$$
$$(39)$$

where $q_j \in \{0, 1\}$ stands for the state of atom j. After this, we measure every atom (in the z-basis). The probability of any resulting sequence, $\mathbf{q} = (q_1, q_2, \ldots q_N) \in \{0, 1\}^{\times N}$, is

$$\mathcal{P}(\mathbf{q}|\Psi'_\phi) = \frac{1}{2^{N+1}} \left[1 + (-1)^{\sum_j q_j} \cos(N\phi)\right], \quad (40)$$

and the probability of the parity, $p = \big(\sum_j q_j\big) \bmod 2$, is

$$\mathcal{P}(p|\Psi'_\phi) = \frac{1 + (-1)^p \cos(N\phi)}{2}, \qquad p \in \{0, 1\}. \quad (41)$$

On the other hand, these probabilities are different when they are conditioned on being in the mixed part of the density matrix.

$$\mathcal{P}(\mathbf{q}|\rho_{\text{mixed}}) = \frac{1}{2^N}, \qquad \mathcal{P}(p|\rho_{\text{mixed}}) = \frac{1}{2} \quad (42)$$

$\forall \mathbf{q} \in \{0, 1\}^{\times N}$ and $\forall p \in \{0, 1\}$, where $\rho_{\text{mixed}} = [|\mathbf{0}\rangle\langle\mathbf{0}| + |\mathbf{1}\rangle\langle\mathbf{1}|]/2$.

The resulting total probability is the weighted sum of the two cases,

$$\mathcal{P}(p|\phi) = c\mathcal{P}(p|\Psi'_\phi) + (1-c)\mathcal{P}(p|\rho_{\text{mixed}}) \quad (43)$$

$$= \frac{1 + c(-1)^p \cos(N\phi)}{2}, \quad (44)$$

where $c = 2F_N - 1$ is the contrast of the interference fringes.

C. Fisher information

We rely on inferring the unknown phase ϕ, from a series of parity measurements, as described above. The

information content (about ϕ) of a single measured value p is quantified by the Fisher information,

$$\mathcal{F}(\phi) = \sum_{p \in \{0,1\}} \mathcal{P}(p|\phi) \left[\ln \frac{d}{d\phi} \mathcal{P}(p|\phi) \right]^2 \qquad (45)$$

$$= N^2 \frac{\sin^2(N\phi)}{1/c^2 - \cos^2(N\phi)}, \qquad (46)$$

where the true value of the phase is ϕ. The average Fisher information is

$$\overline{\mathcal{F}} = \frac{1}{2\pi} \int_{-\pi}^{+\pi} d\phi \, \mathcal{F}(\phi), \qquad (47)$$

which we can evaluate in the limit of $c \ll 1$,

$$\overline{\mathcal{F}} \approx \frac{1}{2\pi} \int d\phi \, c^2 \cos^2(N\phi) = \frac{N^2 c^2}{2}. \qquad (48)$$

In the other limit, when $1 - c \ll 1$, $F(\phi)$ is approximately c^2 everywhere, except near the points where $\sin(N\phi) = 0$. We approximate the dip at $\phi = 0$ with

$$\frac{\sin^2 x}{1/c^2 - \cos^2 x} \approx \frac{x^2}{\frac{1-c^2}{c^2} + x^2}, \qquad \text{where } x = N\phi, \quad (49)$$

and the integral with

$$\frac{\overline{\mathcal{F}}}{N^2} \approx c^2 - \frac{2}{2\pi} \int_{-\pi}^{+\pi} dx \left(1 - \frac{x^2}{\frac{1-c^2}{c^2} + x^2} \right) \qquad (50)$$

$$= c^2 - \frac{\sqrt{1-c^2}}{c} \approx 1 - \sqrt{2(1-c)}, \qquad (51)$$

where we have used that F is periodic with period $2\pi/N$.

Using these two limits for the average Fisher information, we approximate it with

$$\overline{\mathcal{F}} \approx \begin{cases} N^2 c^2/2 & , \quad \text{if } \quad c \le 0.7, \\ N^2 \left(1 - \sqrt{2(1-c)} \right) & , \quad \text{if } \quad 1 - c > 0.7. \end{cases} \qquad (52)$$

The quality of this approximation can be read off from Fig. 4

D. Cramér-Rao bound

The average Fisher information $\overline{\mathcal{F}}$ is a good measure of the posterior uncertainty of the phase ϕ, if the prior distribution of the phase has been previously narrowed down to a small enough interval such that its posterior is single peaked. In case of using the GHZ state, this requires a very narrow prior to start with: $\phi \in [-\pi/N, +\pi/N]$. In our previous work, we showed that this is possible by employing the atoms in a scheme using a series of cascaded GHZ states [4]. The Cramér-Rao bound on the expected deviation of the estimated ϕ from the true one implies

$$\Delta\phi = \sqrt{\langle(\phi_{\text{estimate}} - \phi_{\text{true}})^2\rangle} \ge \left[\nu \overline{\mathcal{F}} \right]^{-1/2}, \qquad (53)$$

where ν is the number of independent repetitions of the measurement. We are going to assume equality to simplify our analysis.
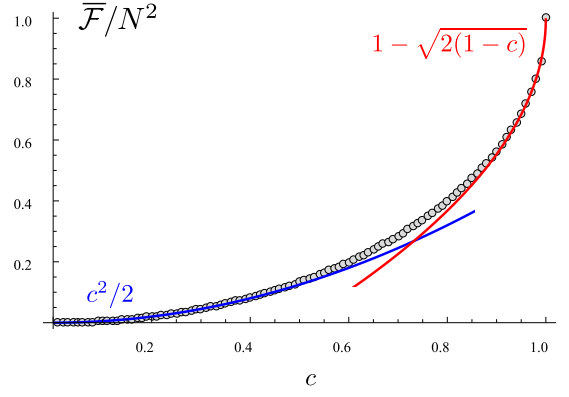

FIG. 4. Average Fisher information as a function of the contrast c (dots). It is well approximation by $c^2/2$ for $c < 0.6$ and by $1 - \sqrt{2(1-c)}$ for $c > 0.8$ (solid curves).

E. Allan deviation

The average fractional frequency uncertainty of an atomic clock (with central frequency ω_0), averaged over a long time period τ, is called Allan deviation [4],

$$\sigma = \frac{(\Delta\omega)_\tau}{\omega_0} \approx \frac{\Delta\phi_t/t}{\omega_0} \frac{1}{\sqrt{\tau/t}} \approx \frac{1}{\omega_0\sqrt{\tau}} \left[\nu t \overline{\mathcal{F}} \right]^{-1/2} \qquad (54)$$

where $(\Delta\omega)_\tau = \left| \frac{1}{\tau} \int d\tau' \, \omega(\tau') - \omega_0 \right|$ is the deviation of the average frequency over time τ, and $\Delta\phi_t$ is the average deviation of the measured phase (from the true one) in a single interrogation of length t. The $\sqrt{\tau/t}$ factor comes from the number of independent repetitions of the same, t-long, interrogation cycle.

In Ref. [5], we showed that σ can reach

$$\sigma_{\text{ent}} \approx \frac{1}{\omega_0 \tau} \frac{8}{\pi} \frac{\sqrt{\log N}}{N}, \qquad (55)$$

if $\tau < \gamma_{\text{at}}^{-1}/N$, the reduced atomic coherence time, and if the contrast is perfect, $(c = 1)$. Using the approximation for $\overline{\mathcal{F}} \approx N^2 c^2/2$, and the fact that $\sigma \propto [\overline{\mathcal{F}}]^{-1/2} \propto c^{-1}$, we can augment this result with a c-dependence, and express the Allan deviation in the presence of imperfections as

$$\sigma_{\text{ent}}^{(\text{imperfect})} = \sigma_{\text{ent}}/c = \frac{1}{c\omega_0\tau} \frac{8}{\pi} \frac{\sqrt{\log N}}{N}. \qquad (56)$$

F. Comparison to non-entangled interrogation

Using the same number of atoms, N, we can arrange a measurement without using any entanglement. This results in the Allan deviation of

$$\sigma_{\text{non-ent}}(\tau) \approx \frac{1}{\omega_0 \tau \sqrt{N}}, \qquad \text{if } \quad \tau < 1/\gamma_{\text{LO}}, \qquad (57)$$

where γ_{LO}^{-1} is the laser coherence time. This, representing the standard quantum limit (SQL), is expected to

be larger than the Allan deviation corresponding to the GHZ state scheme, which is almost at the Heisenberg limit. The precision gain of the GHZ scheme over the non-entangled one is

$$G = \frac{\sigma_{\text{non-ent}}}{\sigma_{\text{ent}}/c} = (2F_N - 1)\frac{\pi}{8}\sqrt{\frac{N}{\log N}}. \qquad (58)$$

Since the fidelity F_N decreases with increasing N, there exist an optimal N_{opt}, for which the gain G is maximal.

G. Optimal clock network size

If each clock runs with the optimal setup (n_{opt}), then the total error per atom, E, is minimal, and the total fidelity can be written as $F_N = \left[1 + e^{-E_{\min}N}\right]/2$. Plugging this into Eq. (58) gives

$$G = e^{-E_{\min}N}\frac{\pi}{8}\sqrt{\frac{N}{\log N}}, \qquad (59)$$

which takes its maximum at $N = N_{\max} \approx \frac{1}{2E_{\min}}$, giving $G_{\max} \approx \frac{\pi}{8}\left[E_{\min}\log\left(\frac{1}{2E_{\min}}\right)\right]^{-1/2}$. In the meantime the number of atoms at a single clock is ~ 2500. As a result the optimal number of clocks becomes

$$K_{\text{opt}} \sim \frac{N_{\max}}{2500}. \qquad (60)$$

On Fig. 5, we plot $N_{\max}$, n_{opt}, and K_{opt} as a function of the principle quantum number of the Rydberg states $\tilde{n}$. For $\tilde{n} = 120$, we find $N_{\max} \approx 15000$ (2D) and $\approx$
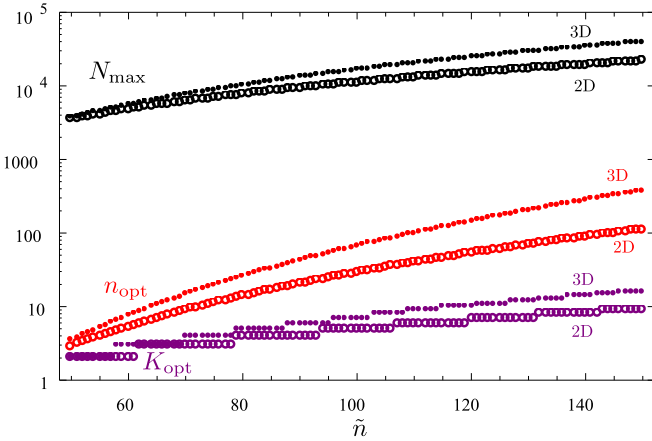
FIG. 5. The optimal total number of entangled atoms in the network $N_{\max}$ and the number of atoms at a single clock n_{opt} as a function of the principle quantum number $\tilde{n}$. The thin dotted lines show the multiples of n_{opt}. The optimal number of clocks, $K_{\text{opt}} \sim N_{\max}/2500$ is written on the corresponding regions of $\tilde{n}$, for the 2D and 3D setup.

25000 (3D). Using the n_{opt} values from before (≈ 50 and

≈ 150), we find $K_{\text{opt}} \sim 6$ and ~ 10, for 2D and 3D, respectively.

With the optimal architecture, we can plot the maximal gain $G_{\max}$ (compared to the non-entangled scheme using the same number of atoms) as a function of principle quantum number $\tilde{n}$. This is shown on Fig. 6. For
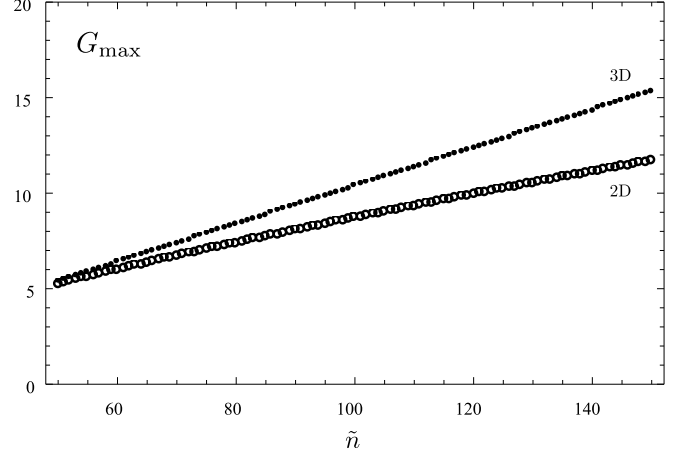
FIG. 6. Maximal gain over the non-entangled scheme provided by the optimal entangled clock network architecture as a function of principle quantum number of the Rydberg states $\tilde{n}$, for the 2D and 3D setup.

$\tilde{n} = 120$, the gain is $G_{\max} = 10$ (2D) and 12 (3D).

VIII. GHZ GENERATION TIMESCALE

The global GHZ state needs to be set up at the beginning of every clock cycle. The average total time required to perform every step successfully is determined by the time it takes the longest step (photon propagation), and how many times this has to be repeated, after heralding indicates (partial) failure.

Ideally photon propagation and classical communication takes $2L/c$ time, where L is the distance between neighboring clocks and c is the speed of light (in the fiber). For clocks separated by 5 km, this is 0.17 μs.

However, the two-photon detection process is probabilistic, which (for distances ~ 5 km) succeeds only every fourth time $p = 1/4$. This means that the probability that a single link still fails to establish after the tth trial is $(1-p)^t$. Conversely, the probability that it succeeds some time before or on the tth trials is $1 - (1-p)^t$. The probability that all $K - 1$ links succeed is $\left[1 - (1-p)^t\right]^{K-1}$, and the probability that at least one of them still didn't succeed in t trails is $1 - \left[1 - (1-p)^t\right]^{K-1}$. Now, this is exactly the probability that we need to try more than t times before globally succeeding. This means we can write the probability of globally succeeding exactly on

the $t$the trial is:

$$\mathcal{P}(t) = \mathcal{P}(\text{no success in } t - 1 \text{ trial})$$
$$- \mathcal{P}(\text{no success in } t \text{ trials}) =$$
$$= \left\{ 1 - \left[1 - (1-p)^{t-1} \right]^{K-1} \right\}$$
$$- \left\{ 1 - \left[1 - (1-p)^{t} \right]^{K-1} \right\} \quad (61)$$

The expectation value of t (number of required repetitions) can be calculated numerically for $p = 0.25$ and $K = 10$ is $\langle t \rangle = 10.33$.

Multiplying the ideal wait time with this expected number of repetitions gives 1.75μs average time required to set up the global GHZ state.

IX. PROSPECTS WITH CURRENT EXPERIMENTAL TECHNOLOGY

In our analysis above, we investigated the effects of noise sources which are fundamental to photons and Rydberg states. This result, however, posits only a lower bound to infidelity. Realizing our scheme with current experimental technology is more challenging than it may seem, due to additional imperfections of the implementation.

Out of the five steps of our protocol, generating the spin-photon entangled states (step 2) and producing the entangled states between neighboring but remote atomic ensembles (step 3) are the most restrictive. Although possible, the overall efficiency is low ($\sim 70\%$ for non-local entangling [6], and $\sim 90\%$ for Rydberg efficiency [7]). This greatly limits the possibility of demonstrating overall precision boost with current experimental technology.

X. CALCULATING $\langle 1/\Delta_{12}^2 \rangle$

Here, we calculate the average of

$$\frac{1}{\Delta_{12}^2} = \left(\frac{\hbar}{C_{12}^{(3)}} \right)^2 |\mathbf{r}_1 - \mathbf{r}_2|^6 \quad (62)$$

for all (j, k) pairs in an ensemble of n atoms, trapped in a (square or cubic)lattice with periodicity a, uniformly filling a circular 2D (spherical 3D) region of radius R.

Averaging over the cloud of atoms, can be approximated by the following integral

$$\left\langle \frac{1}{\Delta_{12}^2} \right\rangle \approx \left(\frac{\hbar}{C_{12}^{(3)}} \right)^2 \underbrace{\frac{1}{V^2} \int_V d^\eta \mathbf{r}_j \int_V d^\eta \mathbf{r}_k |\mathbf{r}_j - \mathbf{r}_j|^6}_{R^6 I} \quad (63)$$

where $\eta = 2, 3$, V is the filled region, of radius R, in a (2D or 3D) lattice.

We introduce new variables $x = |\mathbf{r}_j - \mathbf{r}_k|$, $r = |\mathbf{r}_j|$, and use the circular symmetry of the cloud and the spherical symmetry of the interaction, to turn the integrals into one dimensional ones.

$$R^6 I_{2D} = \frac{1}{(\pi R^2)^2} \int_0^R dr \, 2\pi r \int_0^{2R} dx \, S_R(r, x) x^6, \quad (64)$$

$$R^6 I_{3D} = \frac{1}{(4\pi R^3/3)^2} \int_0^R dr \, 4\pi r^2 \int_0^{2R} dx \, A_R(r, x) x^6, \quad (65)$$

where the weighting factor $S_R(r, x)$ is the length of the segment of a circle of radius x, centered at r distance from the origin that lies inside the 2D cloud of radius R. (See Fig. 7). It can be written as

$$S_R(r, x) = \begin{cases} 2\pi x & , \text{if } x < R - r \\ 0 & , \text{if } R + r < x \\ 2x \arccos\left(\frac{x^2 + r^2 - R^2}{2xr} \right) & , \text{otherwise} \end{cases} \quad (66)$$

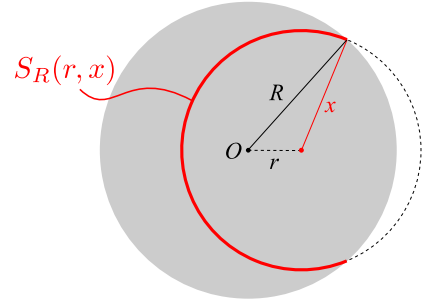Similarly, $A_R(r, x)$ is the area of a spherical surface or

FIG. 7.   The length of the circle segment of radius x lying inside the cloud of radius R, $S_R(r, x)$, is between 0 and $2\pi x$ for $R - r < x < R + r$, where r is the separation between the centers.

radius x centered r distance from the center of the 3D cloud located inside the cloud. It can be written as

$$A_R(r, x) = \begin{cases} 4\pi x^2 & , \text{if } x < R - r \\ 0 & , \text{if } R + r < x \\ \pi \frac{x}{r} \left[R^2 - (x - r)^2 \right] & , \text{otherwise} \end{cases} \quad (67)$$

Using the explicit expressions of Eq. (66) and (67), we

can write

$$I_{2D} = 4 \int\limits_0^1 d\rho\, \rho \int\limits_0^{1-\rho} d\xi\, \xi^7 + \tag{68}$$

$$+4 \int\limits_0^1 d\rho\, \rho \int\limits_{1-\rho}^{1+\rho} d\xi\, \frac{1}{\pi} \xi^7 \arccos\left(\frac{\xi^2 + \rho^2 - 1}{2\rho\xi}\right), \tag{69}$$

$$I_{3D} = 9 \int\limits_0^1 d\rho\, \rho^2 \int\limits_0^{1-\rho} d\xi\, \xi^8 + \tag{70}$$

$$+9 \int\limits_0^1 d\rho\, \rho^2 \int\limits_{1-\rho}^{1+\rho} d\xi\, \frac{1}{4}\frac{\xi^7}{\rho}\left[1 - (\xi - \rho)^2\right], \tag{71}$$

which we numerically evaluate and find $I_{2D} = 3.5$, and $I_{3D} = 4.27$.

Using that $\pi R^2 = na^2$ (in 2D) and $4\pi R^3/3 = na^3$ (in 3D), we can obtain the expressions in Eq. (11).

XI. CALCULATING $\langle 1/\Delta_{12}^2 \rangle$ FOR MESSENGER ATOM

When a messenger atom is used, we imaging placing it just outside the amotic cloud. This changes the expression from Eq. (63) to

$$\left\langle \frac{1}{\Delta_{12}^2} \right\rangle \approx \left(\frac{\hbar}{C_{12}^{(3)}}\right)^2 \frac{1}{V} \int\limits_V d^\eta \mathbf{r}\, |\mathbf{r} - \mathbf{r}_m|^6, \tag{72}$$

where $\mathbf{r}$ is the position of an atom in the cloud, and $\mathbf{r}_m$ is the messenger atom's position. Following the same steps as in the previous section, we need to calculate the following integrals:

$$R^6 J_{2D} = \frac{1}{\pi R^2} \int\limits_0^{2R} dx\, S_R(r_m, x) x^6, \tag{73}$$

$$R^6 J_{3D} = \frac{1}{4\pi R^3/3} \int\limits_0^{2R} dx\, A_R(r_m, x) x^6. \tag{74}$$

Using that $r_m = |\mathbf{r}_m| = R$, and the expressions for S_R and A_R, we get $J_{2D} = 8.75$ and $J_{3D} = 4.27$.

This results in a $\sim$ 2-fold increase of the imperfect blockade error, raising its contribution to 20-30% in the total error, and increasing it by $\sim 10\%$

XII. CALCULATING $\langle 1/\Delta_{11}^2 \rangle$

Following the same line of thoughts as in the previous section, we can write the average as

$$\left\langle \frac{1}{\Delta_{11}^2} \right\rangle = \approx \left(\frac{\hbar}{C_{11}^{(6)}}\right)^2 \frac{1}{V^2} \underbrace{\int\limits_V d^\eta \mathbf{r}_j \int\limits_V d^\eta \mathbf{r}_k\, |\mathbf{r}_j - \mathbf{r}_j|^{12}}_{R^{12} J} \frac{1}{V^2}. \tag{75}$$

The integral J can be evaluated following the same methods as in the previous section, and we obtain $J_{2D} = 61.29$, $J_{3D} = 68.26$.

Using that $\pi R^2 = na^2$ (in 2D) and $4\pi R^3/3 = na^3$ (in 3D), we can obtain the expressions in Eq. (16).

[1] C. W. S. Conover, Phys. Rev. A **84**, 1 (2011).

[2] D.-W. Fang, W.-J. Xie, Y. Zhang, X. Hu, and Y.-Y. Liu, Journal of Quantitative Spectroscopy and Radiative Transfer **69**, 469473 (2001).

[3] A. D. Turker Topcu, arXiv:1505.07152 (2015).

[4] E. M. Kessler, P. Kómár, M. Bishof, L. Jiang, A. S. Sørensen, J. Ye, and M. D. Lukin, Phys. Rev. Lett. **112**, 190403 (2014).

[5] P. Kómár, E. M. Kessler, M. Bishof, L. Jiang, A. S. Sørensen, J. Ye, and M. D. Lukin, Nature Physics **10**, 582 (2014).

[6] G. Vittorini, D. Hucul, I. V. Inlek, C. Crocker, and C. Monroe, Phys. Rev. A **90**, 040302 (2014).

[7] H. Labuhn, S. Ravets, D. Barredo, L. Béguin, F. Nogrette, T. Lahaye, and A. Browaeys, Phys. Rev. A **90**, 023415 (2014).